IEEE Photonics Journal
An IEEE Photonics Society Publication

# Remotely Up-Converted 20-Gbit/s Error-Free Wireless On–Off-Keying Data Transmission at W-Band Using an Ultra-Wideband Photonic Transmitter-Mixer

Volume 3, Number 2, April 2011

F.-M. Kuo
C.-B. Huang
J.-W. Shi
Nan-Wei Chen
H.-P. Chuang
John E. Bowers
Ci-Ling Pan

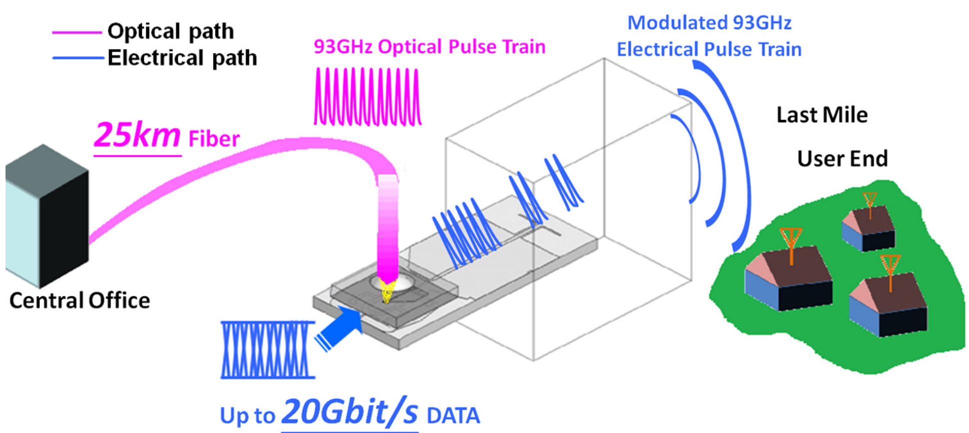


DOI: 10.1109/JPHOT.2011.2126567

# Remotely Up-Converted 20-Gbit/s Error-Free Wireless On–Off-Keying Data Transmission at W-Band Using an Ultra-Wideband Photonic Transmitter-Mixer

**F.-M. Kuo,[1] C.-B. Huang,[2] J.-W. Shi,[1,3] Nan-Wei Chen,[4] H.-P. Chuang,[2] John E. Bowers,[3] and Ci-Ling Pan[2]**

[1]Department of Electrical Engineering, National Central University, Taoyuan 320, Taiwan
[2]Institute of Photonics Technologies, National Tsing-Hua Universit, Hsinchu 300, Taiwan
[3]Electrical and Computer Engineering Department, University of California, Santa Barbara, CA 93106 USA
[4]Department of Communications Engineering, Yuan Ze University, Taoyuan 320, Taiwan

*DOI: 10.1109/JPHOT.2011.2126567*
*1943-0655/$26.00 ©2011 IEEE*

Manuscript received January 27, 2011; revised March 4, 2011; accepted March 5, 2011. Date of publication March 10, 2011; date of current version March 22, 2011. This work was supported by the Ministry of Economic Affairs of Taiwan under Grant 98-EC-17-A-07-S1-001 and the National Science Council of Taiwan under Contract NSC-98-2221-E-008-009-MY3, Contract NSC-97-2112-M-007-025-MY3, and Contract NSC-98-2221-E-007-025-MY3. Corresponding author: J.-W. Shi (e-mail: jwshi@ee.ncu.edu.tw).

**Abstract:** We demonstrate a remotely up-converted and distributed 20-Gbit/s wireless on–off-keying (OOK) data transmission link at the W-band that uses a near-ballistic uni-traveling-carrier photodiode (NBUTC-PD)-based photonic transmitter-mixer. This device consists of an active NBUTC-PD integrated with a planar passive circuit for feeding the intermediate-frequency (IF) modulation input and extracting the up-converted optical-to-electrical (O–E) output signals. An equivalent-circuit model is developed, which allows for the O–E and IF responses to be independently optimized. Accordingly, we can achieve both an ultra-wide O–E bandwidth (67–118 GHz) and IF modulation bandwidth ($>$ 15 GHz) with a very-low coupling loss ($<$ 2 dB) from the NBUTC-PD to the WR-10 waveguide. We adopted a remotely distributed 1-ps optical pulse train source with a repetition rate at 93 GHz to serve as a high-performance photonic carrier, which is generated by a spectral line-by-line shaper utilizing the repetition-rate multiplication (RRM) technique. In contrast to lossy amplitude filtering, our RRM is based on applying periodic loss-less spectral *phase filtering* onto the 31-GHz comb lines. In comparison with the conventional 93-GHz sinusoidal carrier, the photogenerated millimeter-wave (MMW) power of this kind of carrier is 4 dB higher than that of PD under the same output photocurrent. In contrast to the traditional mode-locked laser, the fiber dispersion can be totally precompensated without additional dispersion compensation components. By use of such device and optical MMW source, we successfully demonstrate remotely distributed and up-converted 20-Gbit/s error-free OOK wireless data transmission link over a 25-km standard single-mode fiber.

**Index Terms:** Microwave photonics, photodetectors.

## 1. Introduction

With the development of numerous kinds of multimedia services such as 3-D face-to-face communication [1] and High-Definition Multimedia Interface (HDMI) 1.4 [2], the market demand for data capacity on the scale of tens of gigabits per second has grown rapidly [3]–[5]. Radio-over-Fiber

(RoF) communication systems are considered to be one of the most suitable candidates to meet this demand and to develop the desired ultra-broadband wireless access network [4]–[6]. However, it is still a challenge to acquire sufficient bandwidth for data transmission of tens of gigabits per second over the last mile of such a system. One possible solution to this problem is to enlarge the spectral efficiency of the wireless link to transmit more data over the same bandwidth [4]. However, such a solution calls for a much higher signal-to-noise ratio (SNR) and requires a complex receiver to perform the demodulation/equalization process. Another possible solution is to straightforwardly increase the carrier frequency [5], but this requires photonic transmitters (PTs) with more optical-to-electrical (O–E) bandwidth in order to achieve a higher transmission data rate under the simple on–off-keying (OOK) format. Using such an approach, a research group at Nippon Telegraph and Telephone (NTT) has demonstrated 14-Gbit/s error-free line-of-sight OOK wireless linking at the 300-GHz band simply by using the uni-traveling-carrier photodiode (UTC-PD)-based PTs [5]. However, fiber chromatic dispersion becomes more serious during long-haul distribution when both the millimeter-wave (MMW) carrier frequency and data rate increase as is the case under the conventional RoF scheme [7]. Such a problem leads to serious signal fading and time-shifting effects, and thus limits the maximum fiber transmission distance of RoF systems. Furthermore, in order to transmit multichannel data signals, the conventional RoF system requires more photonic MMW carrier signals at different optical wavelengths. This issue means a considerable occupation of the optical bandwidth when both the MMW carrier frequency and data rate increase. However, the combination of remote signal up-conversion techniques with a nonlinear photodetection scheme provides a promising solution for the aforementioned dispersion problem [7]. The photonic carrier (with fixed optical wavelengths) can thus be shared between different baseband channels in order to save the required optical bandwidth. Ten gigabit-per-second signal generation [8] and 1.25-Gb/s wireless data transmission [9] have been realized through the use of a nonlinear photodetection scheme (bias modulation) with the UTC-PD. Furthermore, by use of the traveling-wave UTC-PD-based optoelectronic mixer, the nonlinear down-conversion experiment at 100 GHz radio frequency (RF), has been successfully achieved [10]. Nevertheless, it seems that the intermediate-frequency (IF) modulation bandwidth ($\sim$7 GHz) of the UTC-PD is limited by its switching speed [8]. This is determined by the required time constant from forward to reverse bias operations [8], which is necessary for enhancing the nonlinearity and extinction ratio of the device during bias modulation. This problem can be overcome with our demonstrated near-ballistic uni-traveling-carrier photodiode (NBUTC-PD) high-performance optoelectronic mixer [11]. The flip-chip bonding packaged NBUTC-PD exhibits extremely high saturation current-bandwidth product (SCBP) performance (37 mA, 110 GHz, 4070 mA-GHz) [12], [13], ultra-wide ($>$ 10 GHz) IF modulation bandwidth (IMB) [11] and high ($>$ 33 dB) extinction ratio during IF modulation [14]. The successful accomplishment of remotely up-converted 12.5-Gbit/s OOK wireless data transmission at the W-band using the NBUTC-PD-based photonic transmitter-mixer (PTM) has been described in our previous work [14]. However, the demonstrated maximum data rate is limited by the IMB, which is around 5 GHz. In this current study, we develop an equivalent-circuit model with a cascade topology to effectively and precisely design a novel PTM module [15], [16]. With this design, we simultaneously achieve an ultra-broadband O–E bandwidth (67–118 GHz, fractional bandwidth $>$ 55.2%), ultra-wide IMB ($>$ 15 GHz), and low ($\sim$2 dB) coupling loss from the NBUTC-PD to the WR-10 waveguide output.

In order to further realize the goal of high-performance data transmission, we also develop a remotely distributed 1-ps optical pulse trains with a repetition rate of 93 GHz to act as synchronized high-performance photonic carrier for wireless data transmission [17]. In this paper, the 93-GHz optical pulse trains are generated through repetition-rate multiplication (RRM) of an initially 31-GHz optical pulse train via a spectral line-by-line shaper. RRM using both amplitude and phase filtering are performed and the results are compared. Further information regarding RRM is provided in Section 3. The photogenerated (at a frequency of 93 GHz) MMW power of this carrier is 4 dB higher than that of PD under the conventional 93-GHz sinusoidal carrier excitation with the same output photocurrent. Such a large improvement means that we may be able to reduce the optical power budget for data transmission while resulting in better PTM reliability with the desired MMW output power.

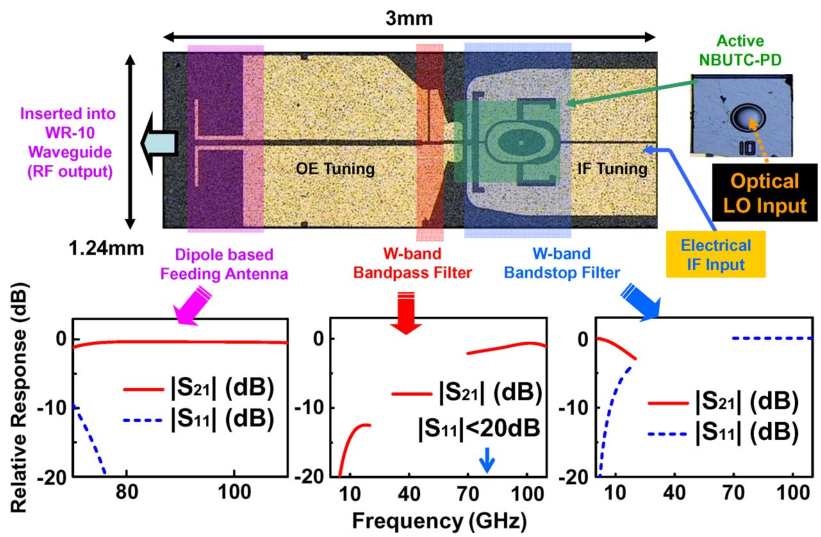


Fig. 1. Top-view of the novel NBUTC-PD-based PTM. The insets give the simulated frequency responses of the scattering (S) parameters of the bandpass filter (BPF), band-stop filter (BSF), and dipole-based feeding antenna (FA).

In the work using mode-locked lasers for remote MMW power enhancement, dispersion compensation must be carefully managed for the delivery of sub-picosecond optical pulses [18]. As a direct comparison, here, we demonstrate that using our photonic MMW source, chromatic dispersion for a long fiber transmission distance of the sub-picosecond optical pulses can be completely precompensated, without the need for additional dispersion compensation components [17]. In our experimental setup, the entire wireless link (after the up/down-conversion process and with a pair of horn antennas) provides a 15-GHz channel bandwidth at the baseband for transmitting an ultra-broadband data signal. The high sensitivity ($>$ 3 kV/W) of the detector and the high-power performance of the NBUTC-PD eliminates the need for W-band MMW amplifiers at both the transmitting and receiving ends of our demonstrated link. Consequently, a remotely distributed and up-converted 20-Gbit/s error-free OOK wireless data transmission link over a 25-km standard single-mode fiber (SSMF) has been demonstrated successfully.

## 2. Device Structure and Fabrication

Fig. 1 shows the top-view of the demonstrated novel NBUTC-PD-based PTM. As can be seen, it is mainly composed of a flip-chip bonded NBUTC-PD with a 100-$\mu$m$^2$ active area, a bandpass filter (BPF), a band-stop filter (BSF), and a dipole-based feeding antenna (FA). The simulated frequency responses of the scattering (S) parameters of these three major passive components (BPF, BSF, and FA) are given in the insets to Fig. 1. As compared with the device described in our previous work [14], the NBUTC-PD active device has a smaller active area (100-$\mu$m$^2$ versus 144-$\mu$m$^2$), which corresponds to a better speed performance (3-dB O–E bandwidth $>$ 200 GHz under a 25 $\Omega$ load) [12] which is important for achieving an ultra-wideband PTM. A slot-line (SL) structure on a 150-$\mu$m thick aluminum nitride (AlN) substrate is employed for the passive circuits due to its good thermal conductivity and reduced substrate mode [15]. As can be seen in the inset to Fig. 1, the FA shows a low coupling loss for feeding the MMW power into the WR-10 waveguide in the full W-band [15], [16]. For details about this component, see our previous work [15], [16]. In order to simultaneously realize a fully integrated PTM module with an ultra-broadband O–E bandwidth, ultra-wide IMB, and low coupling loss from the NBUTC-PD to the WR-10 waveguide output, without accuracy loss, we exploit a relatively efficient cascaded equivalent-circuit model rather than demand the time-consuming full-wave analysis for chip characterization [15], [16]. Technically, the building-block diagram of the entire system is provided in Fig. 2. It is shown that the accurate O–E bandwidth and IMB are obtained with the inclusion of the undesired parasitic effects, especially from

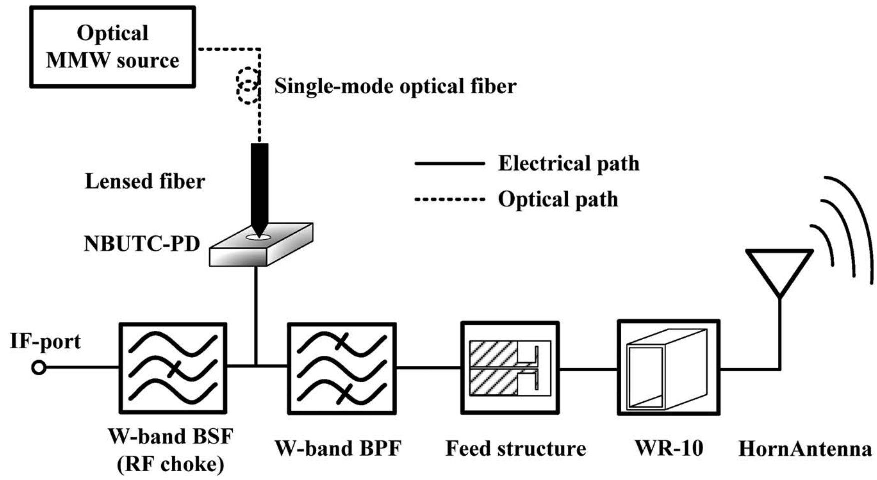


Fig. 2. Schematic system building-block diagram.

the high dielectric constant InP substrate of the NBUTC-PD, as well as flip-chip bonding pillars for heat sinking [15], [16], in the proposed circuit model. In Fig. 2, the function of the passive circuit blocks, i.e., W-band BSF and BPF, is described as follows. In Fig. 2, the IF signal passing through a W-band BSF, which is also termed as the RF choke, is pumped into the NBUTC-PD for the optical MMW source modulation. The modulated W-band source passing through a W-band BPF is then forwarded to the waveguide feed of the horn antenna. Here, the BPF employed herein is for isolation enhancement between the IF port and the waveguide feed structure. In our previous work [15], the partially reflected W-band source from the feed is filtered out by the RF choke regarding the input signal integrity. However, the IF signal is not completely delivered to the PD for bias modulation since a fractional amount of the power leaks to the waveguide feed. With the BPF, the IF power leakage is alleviated. In other words, the isolation between the IF port and the waveguide feed is further enhanced, which leads to a significant improvement on the video bandwidth of the transmitter. Based on the circuit design point of view, the good isolation at both W- and IF bands represents a successful broadband impedance matching. Indeed, as can be seen in Fig. 1, the W-band BSF shows a high reflection (isolation, around 0 dB of $S_{11}$ at the 75–110 GHz frequency) at the W-band and reasonable transmission loss ($S_{21}$ less than $-3$ dB) at the IF band (DC to 15 GHz). On the other hand, the BPF shows reasonable transmission loss ($S_{21} < -3$ dB) at the W-band and a high rejection at the IF band ($S_{21}$ less than $-10$ dB). Hence, this BPF–BSF pair can thus not only separate the RF and IF signals into different flow paths but can also avoid leakage of the injected IF signal and up-converted RF signal to the respective FA and IF input ports of the device. Thanks to this separation, the impedance matching at the O–E and IF bands can be optimized independently and ultra-wide O–E and IF responses can thus be achieved.

## 3. Measurement Results

Fig. 3(a) and (b) illustrate the measurement setup of our NBUTC-PD chip, serving as a PTM module and a flip-chip bonding PD for high-power generation, respectively. In Fig. 3(a) and (b), both NBUTC-PD chips have the same active area of 100 $\mu m^2$. As can be seen in Fig. 3(a), the front-end of the PTM module is inserted into the WR-10 rectangular waveguide for excitation of its fundamental propagation mode. At the same time, the electrical IF and optical local-oscillator (LO) signals are also fed into the PTM module through a microwave probe and lensed fiber, respectively. Note that the full PTM module is suspended in free space to suppress the undesired substrate mode and obtain a low coupling loss [15], [16]. As can be seen in Fig. 3(b), for the case of high-power PD application, the full chip is directly mounted onto the metal chunk for good heat-sinking. A microwave probe is employed in (a) and (b) to feed the IF signal and extract the photogenerated MMW power from the PD, respectively. When we measure the O–E responses of our PTM module,

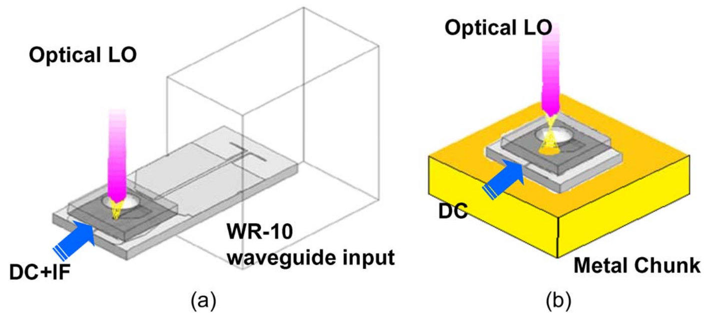


Fig. 3. Experimental setup for measuring the O–E and IF modulation responses of the (a) demonstrated PTM module and (b) the reference flip-chip bonded NBUTC-PD. Different sizes of optical beam waist were used to test our PTM module and PD-chip in (a) and (b), respectively.

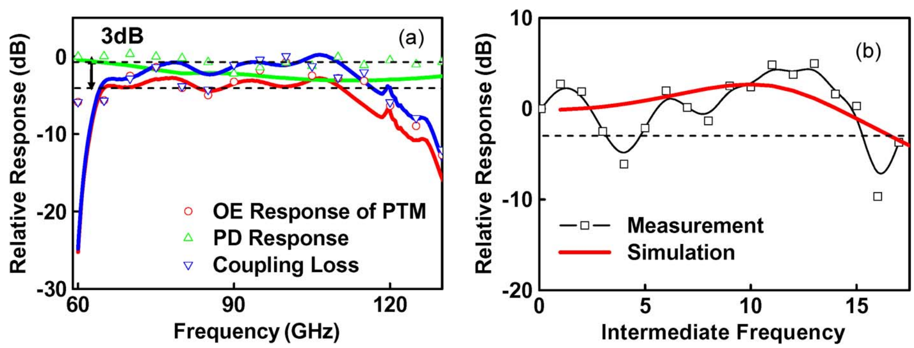


Fig. 4. (a) O–E response of our PTM module, the O–E response of a NBUTC-PD chip with the same active area as (a) under a 50-$\Omega$ load, and the extracted coupling loss from the integrated NBUTC-PD to the WR-10 waveguide output port of the PTM. Note the simulation results of these three traces are also plotted as solid lines. (b) Measured and simulated IF modulation responses of our PTM under 15-mA photocurrent.

the IF input port only provides a fixed DC bias voltage of $-3$ V, while the optical LO frequency is swept from 60 to 130 GHz.

Fig. 4(a) shows plots of the measured and simulated O–E responses of our PTM module, the O–E responses of the flip-chip bonded NBUTC-PD chip under a 50-$\Omega$ load [as shown in Fig. 3(b)], and the coupling loss of the planar dipole-based radiator to the WR-10 waveguide. Here, the 0 dB reference point of all frequency responses shown is defined as the output power from an ideal photodiode (i.e., infinite bandwidth) with a 50-$\Omega$ load, under an ideal sinusoidal optical source excitation (100% modulation depth), and with the same output photocurrent (4 mA) as that of the PTM and PD. The frequency response of the coupling loss, which is defined as the MMW loss from our planar dipole-based FA to WR-10 waveguide, can be extracted by subtracting the measured O–E response for the full PTM module from the measured O–E response for the PD chip. As can be seen, ultra-wide 3-dB bandwidths ($\sim$67–118 GHz, $\sim$53 GHz) can be achieved for both the coupling loss and O–E response with small loss ($<$ 2 dB) with our design. A smaller coupling loss can be expected by further increasing the effective input impedance of our FA to over the 50-$\Omega$ load resistance of the NBUTC-PD chip. Our demonstrated device exhibits a much higher fractional bandwidth ($>$ 55.2%, versus 24.2%) for the O–E response than that of the taper-slot antenna or patch antenna coupled UTC-PD PT [19], [20]. Moreover, the measured O–E responses agree well with the simulation results, which clearly indicate the accuracy of the above model. The IF modulation responses of our PTM under a 15-mA photocurrent are illustrated in Fig. 4(b). During measurement, the injected IF frequency swept from 0.1 to 20 GHz, and the optical LO signal was fixed

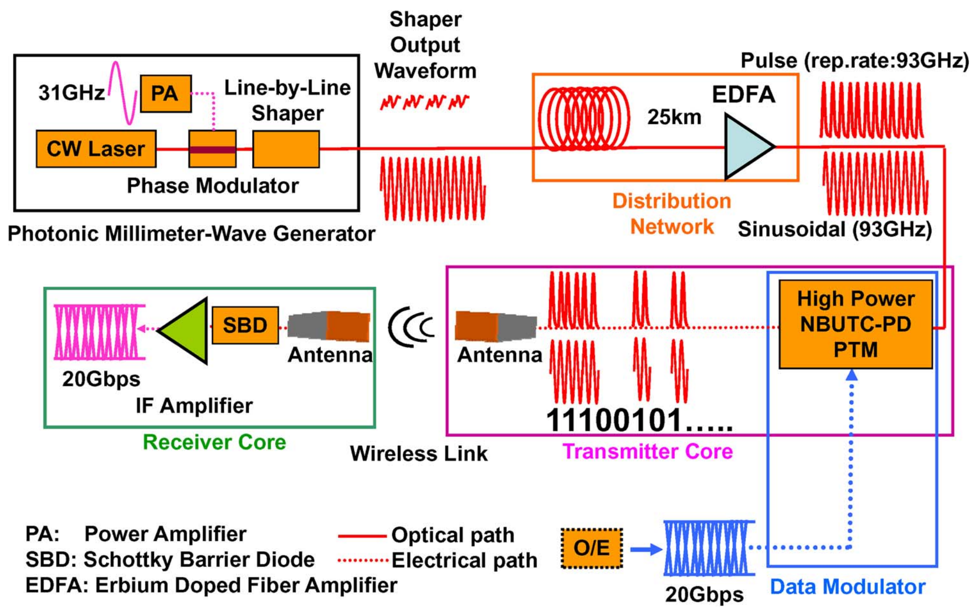


Fig. 5. Experimental setup of our photonic wireless linking system for 20-Gbit/s data transmission by use of line-by-line pulse shaper as photonic MMW source.

at 93 GHz. The waveguide output port of the PTM module was connected to a W-band spectrum analyzer to measure the frequency response of the up-converted RF signal. The peak-to-peak driving voltage $(V_{pp})$ of the input IF signal and DC bias voltage were around 1 V and $-1.9$ V, respectively. Under these operating conditions, clear eye-opening for data transmission could be achieved, to be discussed below. The maximum IMB could exceed 15 GHz, twice the bias modulation bandwidth reported for the UTC-PD [8]. This ultra-wide IMB can be attributed to elimination of forward bias operation of the NBUTC-PD during bias modulation [14] and good broadband impedance matching at the IF band, as described above. In addition, the simulated IF response is well matched to the measured trace, a clear indication of our proposed model for nonlinear IF bias modulation. According to our simulation results, as shown in Fig. 1, the maximum IMB we achieved here is mainly limited by the 3-dB bandwidth of $S_{21}$ of W-band BSF, which shows significant roll-off when the frequency of injected IF signal is over 15 GHz. Overall, the desired ultra-wide O–E bandwidth, ultra-wide IMB, and low coupling loss are all simultaneously achieved in our novel PTM.

In addition, in order to realize high-quality MMW signal generation and wireless data transmission, we also develop a remotely distributed optical short pulse train source with a repetition rate at 93 GHz. Such an optical pulse train is an attractive solution as a synchronized high-performance photonic carrier for wireless data transmission [17], [21]. In comparison to the conventional 93-GHz sinusoidal carrier [22], the pulsed carrier wave exhibits higher (at the 93-GHz frequency) MMW power under the same output photocurrent. Such an improvement is an indication that we may be able to reduce the optical power budget for data transmission. Fig. 5 shows a schematic diagram of the experimental setup for data transmission, including the optical pulse train source. As can be seen, a phase-modulated (PM) continuous-wave (CW) laser frequency comb is generated by injecting a narrow-linewidth CW laser into of a low-$V\pi$ $LiNbO_3$ phase modulator. A 31-GHz sinusoidal signal from an ultra-low phase noise RF signal generator, amplified to $+33$ dBm, is used to drive the phase modulator. A phase modulation frequency of 31 GHz equals the resulting frequency comb line spacing. This will be described later. For details of our line-by-line shaper, see [17] and [21]. By utilizing this setup, $\sim$1-ps optical pulse trains with 31 to 496 GHz repetition rates that are suitable for high modulation-depth photonic MMW generation have been demonstrated [17]. The line-by-line shaper can simultaneously provide accurate dispersion precompensation for delivering short optical pulses to the remote end [17], as illustrated in Fig. 5. This technique can be used to

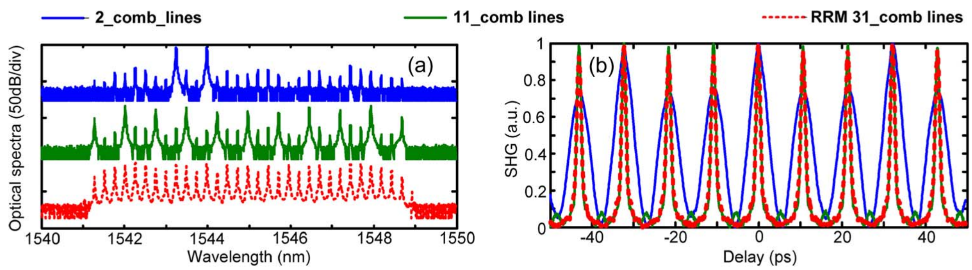


Fig. 6. (a) Optical spectrum and (b) the corresponding experimental intensity autocorrelation (IA) traces of the 93-GHz two comb line sinusoidal signal (amplitude filtering), 93-GHz short-pulse ($\sim$1 ps) signal with 11 comb lines (amplitude filtering), and 93-GHz short-pulse ($\sim$1 ps) signal with 31 comb lines measured using the RRM technique (phase filtering). The initial output spectra of the phase-modulated CW laser are exactly the same as for the 31-comb line signal.

compensate for fiber dispersion during the 25-km-long SSMF delivery. No additional dispersion management need be adopted within the fiber link.

Two possible methods for generating a pulse train with a 93-GHz repetition rate are demonstrated. One is to convert the comb spacing to 93 GHz. This is done by using shaper amplitude filtering on the 31-GHz comb lines. The other method is to apply periodic spectral phase values of $\{0, 2\pi/3, 2\pi/3, \}$ [23] onto the 31-GHz comb lines using the line-by-line shaper. In contrast to lossy amplitude filtering, the phase filtering is a loss-less technique without sacrificing the pulse width, commonly referred to as the temporal Talbot effect [24]. Fig. 6(a) shows the optical spectra for the 93-GHz two comb line sinusoidal signal (amplitude filtering), 93-GHz short-pulse ($\sim$1 ps) signal with 11 comb lines (amplitude filtering), and 93-GHz short-pulse ($\sim$1 ps) signal with 31 comb lines under the RRM technique (phase filtering). Note that the 31-comb line spectra are exactly the same as the initial output of the phase-modulated CW laser. Fig. 6(b) shows the corresponding experimental intensity autocorrelation (IA) traces for these signals. As can be seen, a 27-dB extinction ratio is achieved after amplitude filtering of the undesired comb lines. The 11-comb lines provide a shorter duration of optical power than that of the sinusoidal signal. Thus, we can anticipate a higher MMW output power and an improved signal-to-noise ratio (SNR) from our PT under the same operating current [21]. The amplitude filtered pulse train exhibits almost the same IA traces [same repetition rate and full-width at half-maximum (FWHM)] as with the phase filtered RRM technique without sacrificing the optical comb line power. This benefit can be attributed to accurate phase control of the employed shaper itself. After 25-km SSMF distribution, these optical signals are injected into the aforementioned NBUTC-PD PTM for performing wireless data transmission, as illustrated in Fig. 5. We also tested the high-power performance of our PTM module and NBUTC-PD chip using this high-performance MMW source; see Fig. 3(a) and (b), respectively. The measured bias dependent MMW output power of the PTM versus different numbers of amplitude filtered 93-GHz comb lines under a fixed output photocurrent are plotted in Fig. 7(a). The average photocurrent versus the measured MMW output power of the PTM under 2, 11, and RRM-31 signal illumination is plotted in Fig. 7(b). The ideal line for photogenerated MMW power with a 100% optical modulation depth at a 50-$\Omega$ load is also given for reference. The measurement results are given for an NBUTC-PD module mounted on a metal chunk, as shown in Fig. 3(b), under RRM-31 signal illumination is also shown for reference. It can be seen in Fig. 7(a) that the MMW output power measured under a $-3$ V bias voltage and 4-mA averaged photocurrent exactly increases with the number of 93-GHz comb lines. This phenomenon can be attributed to the reduction of the FWHM which reduces the undesired DC component of the photocurrent, and can be referred to in [21]. The maximum output power is achieved using the 11-comb line pulse source and is 4 dB higher than the conventional two-comb line sinusoidal carrier. Furthermore, an obvious degradation of the output power can be found that when the reverse bias voltage is over the absolute value of $-3$ V. This phenomenon can be attributed to the high electrical field induced carrier drift velocity degradation of electrons in the collector layer of the NBUTC-PD [21]. We can see an over 4-dB enhancement of the short pulse (11 comb and 31 three-times RRM comb) signal under the same bias voltage ($-3$ V) over that of

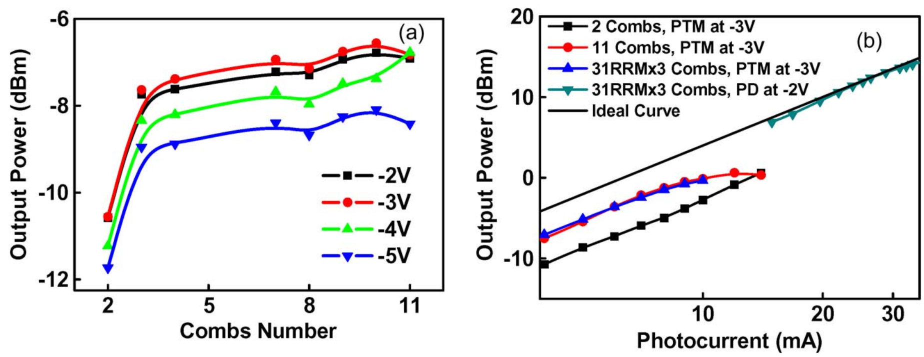


Fig. 7. (a) Measured MMW output power of our PTM versus different numbers of amplitude filtered 93-GHz comb lines under a 4-mA photocurrent and different reverse bias voltages. (b) Measured MMW output power versus photocurrent of our PTM under 2, 11, and RRM-31 signal excitation and that of the reference NBUTC-PD chip under RRM-31 signal excitation. Measurement setups adopted for the PTM module and PD chip are shown in Fig. 2.

the sinusoidal signal (two combs) under a high output photocurrent ($>$ 10 mA). Besides, the high-power performance of the NBUTC-PD chip is superior to that of the PTM module. As can be seen in Fig. 7(b), the relationship between the output power and photocurrent of the reference PD-chip is close to the ideal line and a further 2.7 dB higher than the PTM module under the same photocurrent and the same optical short pulse (31 three-times RRM comb) excitation [25]. Furthermore, the saturation current of the reference PD chip is as high as over 35 mA and three times higher than that of our PTM module. For this comparison, the PD-chip and PTM module is biased under their optimized operation point, i.e., $-2$ V [25] and $-3$ V, respectively, in order to get the highest output RF power. The difference in their optimized bias points can be attributed to that the device-heating problem in PTM module, as discussed latter, would induce significant inert-valley scattering and blur the ballistic transport phenomenon of photogenerated electron. It thus causes that the photo-generated MMW power under $-2$ and $-3$ V is almost the same, as shown in Fig. 7(a). The superior high-power performance of PD-chip to PTM module can be ascribed to the fact that the PD chip is mounted on the metal chunk, which provides much better heat-sinking than for the PTM module suspended in free space for low MMW coupling loss; see Fig. 3. In addition, for high-power measurement of the PD-chip, the lensed fiber is raised to get a more uniform optical field/photocurrent distribution, which should greatly benefit the PDs high-power performance [13], [25], [26]. However, for PTM measurement, the lensed fiber must be almost in contact with the backside of the NBUTC-PD in order to obtain stable light injection. Vibration of the raised lensed fiber will greatly degrade the quality of data transmission. The superior high-power performance of our PD-chip to PTM module is mainly due to the better heat-sinking and more uniform photocurrent distribution in the active area of the PD-chip. We can clearly see that the MMW power delivered by the PD-chip under pulse excitation is close to the ideal line, which is calculated using an optical source with a 100% modulation depth and an ideal PD. The estimated effective modulation depth of our light source is around 160% with a 4-dB enhancement in MMW power, as calculated by de-embedding the around 3-dB high-frequency roll-off in the O–E response of our PD-chip, as shown in Fig. 4(a) [25]. Fig. 5 shows the experimental setup for remote signal up-conversion and wireless data transmission [27], [28]. The 20-Gbit/s data signal used for bias modulation in our PTM can be transmitted by use of the other optical wavelength instead of directly carried on the optical LO signal and then converted to electrical data using another PD at the base station. Thus, we can expect a long fiber transmission distance with less dispersion, as noted above. During the experiments, 20-Gbit/s electrical data is used to directly swing the bias point of the PTM to mimic the case of the aforementioned remote up-conversion [28]. In our system, the receiver end is composed of another W-band horn antenna and a fast power detector (VDI diode) for detecting the envelope of received MMW power, as depicted in Fig. 5. The down-converted data-stream is further amplified, recorded,

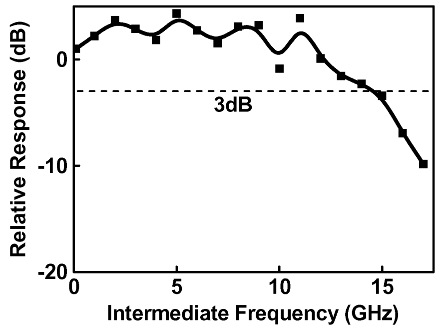


Fig. 8. Measured back-to-back IF frequency responses for the entire channel for wireless data transmission.

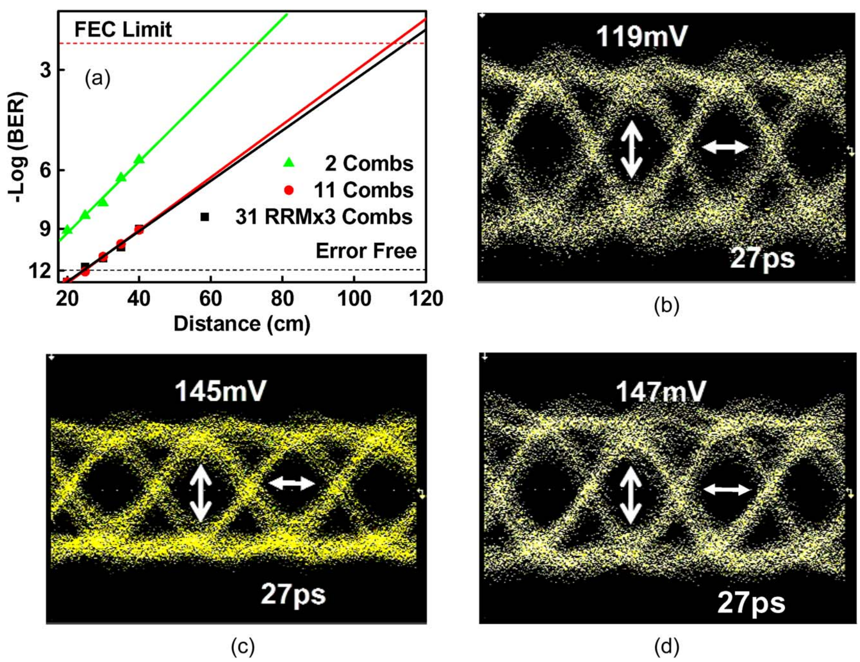


Fig. 9. Measured $-$log (BER) at 20 Gbit/s (PRBS: $2^{15} - 1$) versus transmission distances under three different optical excitation schemes (2, 11, and 31 three-times RRM comb lines). The insets gives the measured 20-Gbit/s eye-patterns for (a) two comb lines, (b) 11 comb lines, and (c) 31 three-times RRM comb lines.

and analyzed by an IF amplifier, high-speed sampling scope, and error-detector, respectively. Fig. 8 shows the measured back-to-back baseband response of the entire channel (after up/down-conversion). The dots in such figure represent the measured data points and the solid curve is just the interconnected lines after smoothing. As can be seen, the baseband bandwidth of the demonstrated channel is around 15 GHz, which may not only be limited by the IMB, as discussed before, but also the video bandwidth of the power detector. Fig. 9(a) shows the $-$log (BER) at 20 Gbit/s (PRBS: $2^{15} - 1$) versus transmission distances measured under three different optical excitations (two, 11 and 31 three-times RRM comb lines). The corresponding 20-Gbit/s eye-patterns are given in Fig. 9(b)–(d). As can be seen, error-free 20-Gbit/s operations are achieved for a 20-cm wireless distance, 25-km fiber transmission distance, and optical short pulse (both 11 and 31 three-times RRM comb lines) excitation. Furthermore, the short pulse excitation offers a lower BER compared with the sinusoidal signal excitation, due to the improved MMW output power performance, as shown in Fig. 7. The significant improvement in 20-Gbit/s BER performance compared with our previous results [27] can be attributed to the increase in the bandwidth of the receiver (fast power detector) and output power performance of our PTM under pulse excitation. A comparison is made with the reported 16-QAM, OFDM, or differential phase shift keying (DPSK) modulation formats [4], [29], [30]. The reported OOK modulation formats here although having extremely high transmission data rates (20 Gbit/s) will have more serious problems with the multipath effect and occupy a larger bandwidth for the same desired data rate. However, we just need a receiver with much more compact and simpler architecture for OOK data detection. By use of the advanced InP-HEMT foundry, the complex modulation and de-modulation processes for 10-Gbit/s quadrature phase shift keying (QPSK) data in a single chip for 125-GHz wireless transmission has been demonstrated [31]. Compared with the reported OOK 10-Gbit/s data transmission [9], this solution offers the same (10 Gbit/s) data rate with only one half the wireless bandwidth and reduced multipath effect and offers a compact size of receiver. The progress in high-speed IC technology thus provides an effective way to optimize tradeoffs between the total transmission data rate, occupied wireless bandwidth, multipath effect, and the size of transreceiver module in the photonic wireless linking system.

## 4. Conclusion

In conclusion, in this work, we demonstrate an NBUTC-PD-based PTM with an extremely wide O–E bandwidth (67–118 GHz) and very-high IMB ($>$ 15 GHz). Thanks to the isolation of the IF modulation input and O–E output signals, and the accuracy of the adopted equivalent-circuit model, both the O–E and IF modulation responses can be precisely optimized. Low coupling loss ($<$ 2 dB) at the W-band from the planar dipole-based radiator to the WR-10 waveguide output port, and a high extinction ratio ($>$ 33 dB) during IF modulation can also be simultaneously achieved. With this novel device 20-Gbit/s error-free OOK wireless OOK data transmission has been successfully achieved over a 25-km-long SSMF, with a dispersion precompensated high modulation depth (160%), short optical pulse ($\sim$1 ps) train, and an ultra-high repetition rate (93 GHz).

## References


[1] T. Yamada, M. Kano, K. Yamamoto, K. Hirota, and M. Hirose, "Multimedia virtual laboratory on the gigabit network," in *Proc. Int. Conf. Artif. Real Telexistence*, Taipei, Taiwan, Oct. 25–27, 2000, vol. 10, pp. 98–103.

[2] HDMI Licensing, LLC, Sunnyvale, CA. [Online]. Available: http://www.hdmi.org/index.aspx

[3] K. Kawasaki, Y. Akiyama, K. Komori, M. Uno, H. Takeuchi, T. Itagaki, Y. Hino, Y. Kawasaki, K. Ito, and A. Hajimiri, "A millimeter-wave intra-connect solution," in *ISSCC Dig. Tech. Papers*, San Francisco, CA, Feb. 7–11, 2010, pp. 414–416.

[4] W. J. Jiang, C. T. Lin, L. Y. Wang He, C. C. Wei, C. H. Ho, Y. M. Yang, P. T. Shih, J. Chen, and S. Chi, "32.65-Gbps OFDM RoF signal generation at 60 GHz employing an adaptive I/Q imbalance correction," presented at the 36th Eur. Conf. Optical Commun., Torino, Italy, Sep. 19–23, 2010, Paper Th.9.B.5.

[5] T. Nagatsuma, T. Takada, H.-J. Song, K. Ajito, N. Kukutsu, and Y. Kado, "Millimeter- and THz-wave photonics towards 100-Gbit/s wireless transmission," presented at the IEEE Photonic Society's 23rd Annu. Meeting, Denver, CO, Nov. 7–11, 2010, Paper WE4.

[6] M. J. Crisp, S. Sabesan, R. V. Penty, and I. H. White, "Radio over fiber distributed antenna networks," *IEEE LEOS Newslett.*, vol. 23, no. 1, pp. 16–20, Feb. 2009.

[7] H.-C. Chien, A. Chowdhury, Z. Jai, Y.-T. Hsueh, and G.-K. Chang, "Long-reach 60-GHz Mm-wave optical-wireless access network using remote signal regeneration and upconversion," in *Proc. 34th ECOC*, Brussels, Belgium, Sep. 21–25, 2008, pp. 137–138.

[8] A. Hirata, T. Furuta, H. Ito, and T. Nagatsuma, "10-Gb/s millimeter-wave signal generation using photodiode bias modulation," *J. Lightw. Technol.*, vol. 24, no. 4, pp. 1725–1731, Apr. 2006.

[9] A. Hirata, T. Minotani, and T. Nagatsuma, "Millimeter-wave photonics for 10-Gbit/s wireless links," in *Proc. IEEE LEOS Annu. Meeting*, Glasgow, U.K., Nov. 10–14, 2002, vol. 2, pp. 477–478.

[10] E. Rouvalis, M. J. Fice, C. C. Renaud, and A. J. Seeds, "Optoelectronic detection of millimetre-wave signals with travelling-wave uni-travelling carrier photodiodes," *Opt. Express*, vol. 19, no. 3, pp. 2079–2084, Jan. 2011.

[11] J.-W. Shi, Y.-S. Wu, and Y.-S. Lin, "Near-ballistic uni-traveling-carrier photodiode based V-band optoelectronic mixers with internal up-conversion-gain, wide modulation bandwidth, and very high operation current performance," *IEEE Photon. Technol. Lett.*, vol. 20, no. 11, pp. 939–941, Jun. 2008.

[12] Y.-S. Wu and J.-W. Shi, "Dynamic analysis of high-power and high-speed near-ballistic uni-traveling carrier photodiodes at W-band," *IEEE Photon. Technol. Lett.*, vol. 20, no. 13, pp. 1160–1162, Jul. 2008.

[13] J.-W. Shi, F.-M. Kuo, C.-J. Wu, C. L. Chang, C. Y. Liu, C.-Y. Chen, and J.-I. Chyi, "Extremely high saturation current-bandwidth product performance of a near-ballistic uni-traveling-carrier photodiode with a flip-chip bonding structure," *IEEE J. Quantum Electron.*, vol. 46, no. 1, pp. 80–86, Jan. 2010.
[14] F.-M. Kuo, H. Yen-Lin, J.-W. Shi, N.-W. Chen, W.-J. Jiang, C.-T. Lin, J. Chen, C.-L. Pan, and S. Chi, "12.5-Gb/s wireless data transmission by using bias modulation of NBUTC-PD based W-band photonic transmitter-mixer," presented at the Optical Fiber Commun., San Diego, CA, Mar. 21–26, 2010, Paper OThF7.
[15] H.-J. Tsai, N.-W. Chen, F.-M. Kuo, and J.-W. Shi, "Front-end design of W-band integrated photonic transmitter with wide optical-to-electrical bandwidth for wireless-over-fiber application," in *Proc. IEEE Microw. Theory Tech. Int. Microw. Symp.*, Anaheim, CA, May 23–28, 2010, pp. 740–743.
[16] N.-W. Chen, H.-J. Tsai, F.-M. Kuo, and J.-W. Shi, "High-speed W-band integrated photonic transmitter for radio-over-fiber applications," *IEEE Trans. Microw. Theory Tech.*, vol. 59, 2011, to be published.
[17] H.-P. Chuang and C.-B. Huang, "Generation and delivery of 1-ps optical pulses with ultrahigh-rates over 25 km single mode fiber by a spectral line-by-line pulse shaper," *Opt. Express*, vol. 18, no. 23, pp. 24 003–24 011, Nov. 2010.
[18] A. Hirata, M. Harada, and T. Nagatsuma, "120-GHz wireless link using photonic techniques for generation, modulation, and emission of millimeter-wave signals," *J. Lightw. Technol.*, vol. 21, no. 10, pp. 2145–2153, Oct. 2003.
[19] A. Hirata, T. Kosugi, N. Meisl, T. Shibata, and T. Nagatsuma, "High-directivity photonic emitter using photodiode module integrated with HEMT amplifier for 10-Gbit/s wireless link," *IEEE Trans. Microw. Theory Tech.*, vol. 52, no. 8, pp. 1843–1850, Aug. 2004.
[20] H. Ito, T. Ito, Y. Muramoto, T. Furuta, and T. Ishibashi, "Rectangular waveguide output unitraveling-carrier photodiode module for high-power photonic millimeter-wave generation in the F-band," *J. Lightw. Technol.*, vol. 21, no. 12, pp. 3456–3462, Dec. 2003.
[21] F.-M. Kuo, J.-W. Shi, H.-C. Chiang, H.-P. Chuang, H.-K. Chiou, C.-L. Pan, N.-W. Chen, H.-J. Tsai, and C.-B. Huang, "Spectral power enhancement in a 100-GHz photonic millimeter-wave generator enabled by spectral line-by-line pulse shaping," *IEEE Photon. J.*, vol. 2, no. 5, pp. 719–727, Oct. 2010.
[22] R. W. Ridgway and D. W. Nippa, "Generation and modulation of a 94-GHz signal using electrooptic modulator," *IEEE Photon. Technol. Lett.*, vol. 20, no. 8, pp. 653–655, Apr. 2008.
[23] C.-B. Huang and Y. C. Lai, "Loss-less pulse intensity repetition-rate multiplication using optical all-pass filtering," *IEEE Photon. Technol. Lett.*, vol. 12, no. 2, pp. 167–169, Feb. 2000.
[24] J. Azaña and S. Gupta, "Complete family of periodic Talbot filters for pulse repetition rate multiplication," *Opt. Express*, vol. 14, no. 10, pp. 4270–4279, May 2006.
[25] C.-B. Huang, J.-W. Shi, F.-M. Kuo, H.-P. Chuang, and C.-L. Pan, "Green and high-power photonic millimeter-wave (MMW) generator for remote generation at 124-GHz," presented at the Optical Fiber Commun., Los Angeles, CA, Mar. 6–10, 2011, Paper OThG6.
[26] M. Chtioui, A. Enard, D. Carpentier, S. Bernard, B. Rousseau, F. Lelarge, F. Pommereau, and M. Achouche, "High-performance uni-traveling-carrier photodiodes with a new collector design," *IEEE Photon. Technol. Lett.*, vol. 20, no. 13, pp. 1163–1165, Jul. 2008.
[27] J.-W. Shi, F.-M. Kuo, H. J. Tsai, Y.-M. Hsin, N.-W. Chen, H.-C. Chiang, H.-P. Chuang, C.-B. Huang, and C.-L. Pan, "20-Gb/s on–off-keying wireless data transmission by using bias modulation of NBUTC-PD based W-band photonic transmitter-mixer," presented at the IEEE Int. Topical Meeting Microwave Photon., Montreal, QC, Canada, Oct. 5–8, 2010, Paper WE3-3.
[28] F.-M. Kuo, J.-W. Shi, N.-W. Chen, C.-B. Huang, H.-P. Chuang, H.-J. Tsai, and C.-L. Pan, "20-Gb/s error-free wireless transmission using ultra-wideband photonic transmitter-mixer excited with remote distributed optical pulse train," presented at the Optical Fiber Commun., Los Angeles, CA, Mar. 6–10, 2011, Paper OWT5.
[29] M. Weiss, A. Stöhr, F. Lecoche, and B. Charbonnier, "27 Gbit/sec photonic wireless 60 GHz transmission system using 16-QAM OFDM," in *Proc. IEEE Int. Topical Meeting Microw. Photon.*, Valencia, Spain, Oct. 14–16, 2009, pp. 1–3 (post deadline).
[30] R.-W. Ridgway, D.-W. Nippa, and S. Yen, "Data transmission using differential phase-shift keying on a 92 GHz carrier," *IEEE Trans. Microw. Theory Tech.*, vol. 58, no. 11, pp. 3117–3126, Nov. 2010.
[31] H. Takahashi, T. Kosugi, A. Hirata, K. Murata, and N. Kukutsu, "10-Gbit/s quadrature phase-shift-keying modulator and demodulator for 120-GHz-band wireless links," *IEEE Trans. Microw. Theory Tech.*, vol. 58, no. 12, pp. 4072–4078, Dec. 2010.